The Peptide Hormone Receptor CEPR1 Functions in the Reproductive Tissue to Control Seed Size and Yield[1][OPEN]

Michael Taleski,[a] Kelly Chapman,[a] Nijat Imin,[b] Michael A. Djordjevic,[a,2] and Michael Groszmann[a,c,3]

[a]Division of Plant Sciences, Research School of Biology, College of Science, Australian National University, Canberra, Australian Capital Territory 2601, Australia
[b]School of Biological Sciences, University of Auckland, Auckland 1010, New Zealand
[c]Australian Research Council Centre of Excellence for Translational Photosynthesis, Division of Plant Sciences, Research School of Biology, Australian National University, Acton, Australian Capital Territory 2601, Australia

ORCID IDs: 0000-0002-4234-6750 (M.T.); 0000-0003-2762-908X (K.C.); 0000-0002-4060-1316 (N.I.); 0000-0002-9819-1372 (M.A.D.); 0000-0002-5015-6156 (M.G.)

The interaction of C-TERMINALLY ENCODED PEPTIDES (CEPs) with CEP RECEPTOR1 (CEPR1) controls root growth and development, as well as nitrate uptake, but has no known role in determining yield. We used physiological, microscopic, molecular, and grafting approaches to demonstrate a reproductive tissue-specific role for *CEPR1* in controlling yield and seed size. Independent Arabidopsis (*Arabidopsis thaliana*) *cepr1* null mutants showed disproportionately large reductions in yield and seed size relative to their decreased vegetative growth. These yield defects correlated with compromised reproductive development predominantly in female tissues, as well as chlorosis, and the accumulation of anthocyanins in *cepr1* reproductive tissues. The thinning of competing reproductive organs to improve source-to-sink ratios in *cepr1*, along with reciprocal bolt-grafting experiments, demonstrated that CEPR1 acts locally in the reproductive bolt to control yield and seed size. *CEPR1* is expressed throughout the vasculature of reproductive organs, including in the chalazal seed coat, but not in other seed tissues. This expression pattern implies that CEPR1 controls yield and seed size from the maternal tissue. The complementation of *cepr1* mutants with transgenic *CEPR1* rescued the yield and other phenotypes. Transcriptional analyses of *cepr1* bolts showed alterations in the expression levels of several genes of the CEP-CEPR1 and nitrogen homeostasis pathways. This transcriptional profile was consistent with *cepr1* bolts being nitrogen deficient and with a reproductive tissue-specific function for CEP-CEPR1 signaling. The results reveal a local role for CEPR1 in the maternal reproductive tissue in determining seed size and yield, likely via the control of nitrogen delivery to the reproductive sinks.

Leucine-rich repeat receptor-like kinases (LRR-RLKs) are one of the largest gene families in plants, comprising more than 220 members in Arabidopsis (*Arabidopsis thaliana*; Gou et al., 2010). Research over the past decade has implicated LRR-RLKs and their selective interactions with secreted peptide hormones in myriad developmental processes, including reproduction, chemotropism, biotic and abiotic stress tolerances, symbiosis, root architecture, regulation of organ number, stomatal function and development, abscission, and general interactions with the environment (Czyzewicz et al., 2013; Delay et al., 2013a; Djordjevic et al., 2015; Santiago et al., 2016; Shabala et al., 2016; Shinohara et al., 2016; Imin et al., 2018; Roy et al., 2018; Chapman et al., 2020).

A conserved LRR-RLK with a growing list of important roles is C-TERMINALLY ENCODED PEPTIDE RECEPTOR1 (CEPR1) in Arabidopsis and its functional ortholog COMPACT ROOT ARCHITECTURE2 (CRA2) in *Medicago truncatula*. In Arabidopsis, CEPR1's ectodomain specifically interacts with peptide hormones of the C-TERMINALLY ENCODED PEPTIDE (CEP) family (Tabata et al., 2014). Arabidopsis has 12 canonical CEP genes, each encoding one or more conserved 15-amino acid CEP domains from which the secreted, mature CEP peptide hormones are derived (Ogilvie et al., 2014). Since the identification of CEPR1 as a CEP receptor (Tabata et al., 2014), its developmental and physiological role has been defined primarily in the context of roots. For example, CEP-CEPR1/CRA2 signaling controls the extent of root growth and development, root nodule number in legumes, and nitrate uptake in roots (Tabata et al., 2014;

Mohd-Radzman et al., 2016; Roberts et al., 2016; Taleski et al., 2016, 2018; Chapman et al., 2019, 2020; Delay et al., 2019). Grafting and split-root studies show that CEPR1 influences nitrate uptake in Arabidopsis via a systemic mechanism and that the rate of nitrate uptake is reduced in *cepr1-1* (Tabata et al., 2014). The identification of mature CEPs in the xylem streams of various plants also supports the existence of systemic mechanisms (Tabata et al., 2014; Okamoto et al., 2015; Patel et al., 2018). The interaction of the root-derived CEPs with CEPR1 in the shoot vasculature triggers the up-regulation of phloem-mobile shoot-to-root signals, namely the glutaredoxins CEP DOWNSTREAM1 (CEPD1) and CEPD2, that up-regulate the level of nitrate transporter expression in roots selectively exposed to high nitrate (Ohkubo et al., 2017). Recently, we demonstrated that local and systemic CEP-CEPR1 signaling curtails the expenditure of resources to control lateral root growth in response to elevated shoot-derived carbon (Chapman et al., 2019) and that systemic CEP-CEPR1 signaling controls aspects of root system architecture in soil (Chapman et al., 2020). CEP-CEPR1 signaling also controls main root growth in Arabidopsis (Delay et al., 2013b, 2019). In *M. truncatula*, CRA2 controls root nodulation systemically from the shoot; however, a local interaction of CEPs with CRA2 controls the growth of lateral roots (Huault et al., 2014; Mohd-Radzman et al., 2015; Laffont et al., 2019).

Whether CEP-CEPR1 signaling plays a role in the growth of shoots has not been thoroughly explored. Aboveground, the *cepr1-1* mutant has been described as dwarfed, producing smaller rosettes with pale green leaves and a shorter floral stem that overaccumulates anthocyanins (Bryan et al., 2012; Tabata et al., 2014). Since these traits are typical responses to nitrogen deficiency (Vidal and Gutiérrez, 2008; Takatani et al., 2014), it could be reasonable to dismiss any *cepr1* aboveground defects as simply the result of reduced nitrate acquisition by the *cepr1* roots. Our anecdotal observations of two *cepr1* null mutants, however, indicated that their yield was reduced much more dramatically than expected based on their modest reduction in vegetative growth. In addition, we observed that the *cepr1* mutants produced smaller seeds. These phenotypes appear inconsistent with an effect of CEPR1 on nitrate uptake alone, given that wild-type plants grown at low nitrogen, or mutants with impaired nitrate uptake, produce normally sized but fewer seeds such that their yield losses are proportional to the decreases in vegetative growth (Schulze et al., 1994; Masclaux-Daubresse and Chardon, 2011).

In contrast to plants with impaired root nitrate uptake, an impairment in the remobilization of assimilated nitrogen from vegetative to reproductive tissues leads to a reduction in both seed size and yield (Guan et al., 2015; Li et al., 2015; Di Berardino et al., 2018; Moison et al., 2018). Smaller seeds also result from knocking out particular USUALLY MULTIPLE ACIDS MOVE IN AND OUT TRANSPORTERS (UMAMIT) genes, which encode transporters required for delivering assimilated nitrogen to seeds (Müller et al., 2015). It is not known if CEPR1 signaling affects nitrogen mobilization and delivery to reproductive sinks; however, the phenotypic similarities of *cepr1* with mutants impaired in these processes hint at this possibility and suggest that CEPR1's control over seed size and yield extends beyond its influence over root nitrate uptake. Supporting this hypothesis, we noted that several Arabidopsis CEPs are expressed in reproductive tissues (Roberts et al., 2013) and that rice (*Oryza sativa*) CEPs *OsCEP5* and *OsCEP6* are specifically expressed at defined stages of reproductive development (Ogilvie et al., 2014; Sui et al., 2016). *CEPR1* is expressed throughout the shoot and root vasculature (Bryan et al., 2012; Huault et al., 2014; Tabata et al., 2014), suggesting roles in multiple tissues.

To explore a potential role for CEP-CEPR1 signaling in reproduction, we addressed several questions. First, what is the physiological basis for yield reduction in *cepr1* mutants? Second, can yield losses in *cepr1* be restored by complementation with transgenic *CEPR1* or by manipulating nutrient allocation from the vegetative tissues? Third, is *CEPR1* expressed in reproductive tissues, and is its effect on yield controlled systemically via vegetative tissues or locally in reproductive tissues? Finally, does CEPR1 regulate genes involved in nitrogen homeostasis/nutrient mobilization in the reproductive tissues?

In this study, we demonstrate that CEPR1 has a specific role in reproductive tissues in the promotion of fecundity, seed yield, and size. The two *cepr1* knockout mutants showed yield reductions of between 88% and 98%, which were associated with the production of smaller seeds and a diminished number of reproductive units. These yield defects correlated with poorly developed reproductive tissues as well as chlorosis and the accumulation of anthocyanins in *cepr1* reproductive tissues, all of which could be restored by transgenic complementation with *CEPR1*. Bolt grafting and manipulation of nutrient allocation to reproductive sinks showed that local CEP-CEPR1 signaling underpins the poor fecundity of the *cepr1* mutants. We found that *CEPR1* expression in the reproductive organs occurred specifically in the vasculature. Notably, *CEPR1* expression in the seed was restricted to the chalazal seed coat, the site where nutrients for seed filling are unloaded from the terminating maternal vasculature (Müller et al., 2015). This result supported a local role for *CEPR1* in the control of seed size and yield through activity in the mother tissue. Finally, we used transcriptional profiling of key marker genes to demonstrate a perturbation of nitrogen status in *cepr1* bolts. Collectively, the results reveal a role for CEP-CEPR1 signaling that involves local activity in the bolt to control nitrogen mobilization and delivery to reproductive sinks.

RESULTS

CEPR1 Controls Vegetative Growth, Reproductive Development, and Seed Yield

We explored whether *CEPR1* plays a role in vegetative and reproductive development by examining two

independent knockout mutant alleles in the Nossen (No-0) and Columbia (Col-0) backgrounds (*cepr1-1* and *cepr1-3*, respectively; Tabata et al., 2014; Chapman et al., 2019). Both *cepr1* knockout mutants displayed an ~30% retardation in rosette growth (Fig. 1, A–C). Since vegetative leaves mobilize resources to the bolt and other reproductive tissues, we examined whether the loss of *CEPR1* function affected yield. The *cepr1* mutants displayed a reduction in the growth of reproductive tissues (Fig. 1, D and E), and the number of reproductive units (siliques, flowers, and buds) on the main inflorescence was reduced by ~10% in *cepr1-1* and ~40% in *cepr1-3* (Supplemental Fig. S1). The diminished reproductive capacity correlated with a substantial reduction in the total seed yield per plant of ~88% and ~98% in *cepr1-1* and *cepr1-3*, respectively (Fig. 1, F and G). The reduced seed yield resulted from a lower seed number and a 12% to 25% reduction in seed weight (Fig. 1, H and I). In general, the limited seeds produced by the *cepr1* mutants were smaller and more diverse in size compared with wild-type seeds (Fig. 1, J and K). These results demonstrate that *CEPR1* knockout reduces vegetative growth as well as seed size and yield.

CEPR1 Activity Controls the Proper Development of Reproductive Organs

The severe reductions in *cepr1* seed yield (~88%–98%) seemed disproportionate to the decrease in vegetative growth (~30%) and the reduced number of reproductive units per main inflorescence (~10%–40%). Therefore, we examined if *CEPR1* knockout mutants had additional effects on reproductive development. An examination of floral development in the *cepr1* mutants (Fig. 2) revealed chlorosis in the sepals of the developing buds and those of the open flowers (Fig. 2, A–H) and anthocyanin accumulation in the apical region of the main stem, pedicle, and valves of the siliques, especially in *cepr1-3* (Fig. 2, E–H). This anthocyanin accumulated in the *cepr1* silique valves shortly after fertilization (stage 14; Smyth et al., 1990), intensified during silique elongation (stages 15–17), and subsided as the silique reached full length (late stage 17; Fig. 2, E–H).

We examined the preanthesis floral structure in dissected stage 12 flowers of wild-type No-0 and *cepr1-1* (Fig. 2, I and J). The *cepr1-1* flowers were smaller than wild-type No-0 but retained the relative dimensional ratios between the different floral organs. There was a clear differentiation of the substructures of the *cepr1-1* gynoecium (i.e. stigma, style, valves, and replum), but, like the sepals, these tissues were chlorotic compared with wild-type No-0 (Fig. 2J). Postanthesis *cepr1-1* flowers (stage 13) were smaller and chlorotic compared with wild-type No-0, but the anthers still elongated and deposited pollen on the stigma similarly to wild-type No-0 (Fig. 2, M and N).

Floral development in the Col-0 *cepr1-3* mutant was impaired more severely than in the No-0 mutant, and it was not possible to determine floral stage by

the conventional landmark developmental events (Smyth et al., 1990). Instead, we determined floral buds equivalent to wild-type Col-0 stage 12, based on the relative position of the bud within the inflorescence from the most recent anthesed flowers. Although the *cepr1-3* sepals were of similar size to those of Col-0, there was a severe underdevelopment of the organs in the inner whorls (Fig. 2, K and L). The *cepr1-3* gynoecium was typically pear shaped and stunted, with a translucent appearance (Fig. 2L). In *cepr1-3*, the petals expanded and the anthers elongated and dehisced; however, the stunting of the gynoecium resulted in a state of near hercogamy (i.e. reduced self-pollination; Fig. 2, O and P). We observed only occasional deposition of *cepr1-3* pollen from the shorter medial stamens onto the poorly developed stigma. Collectively, these results show that loss of *CEPR1* activity perturbs floral and reproductive organ development, with the impact being more severe in Col-0 *cepr1-3* compared with No-0 *cepr1-1*. This suggests that background genetic differences between the Col-0 and No-0 accessions modify the severity of the reproductive development defects resulting from a *CEPR1* knockout.

CEPR1 Positively Influences Seed Yield on a per Silique Basis

Since the loss of *CEPR1* function affected flower development, we investigated whether there were effects on yield per silique in *cepr1* (Fig. 3). First, we assessed siliques of self-pollinated plants and observed that *cepr1* mutants had a higher incidence of unfertilized ovules and of seeds that had aborted at various stages of development (Fig. 3, A and B). The reduction in seed set per silique was particularly severe in *cepr1-3* and worsened acropetally. Therefore, we quantified seed set across silique positions (Fig. 3, C and D). In wild-type No-0, seed set steadily improved with increasing silique positions up the stem, reaching a maximum at approximately silique 14 (Fig. 3C). The *cepr1-1* mutant also showed an improving seed set with increasing silique position up the main shoot, albeit at a decreased rate compared with wild-type No-0. Maximum seed set in *cepr1-1* was lower compared with wild-type No-0 (Fig. 3C). Seed set in wild-type Col-0 was minimal in the first silique and increased to a maximum at approximately silique 6 (Fig. 3D). In contrast to wild-type Col-0, *cepr1-3* had maximal seed set in the first silique, which decreased with increasing silique position (Fig. 3D). We observed nil seed set from silique number 12 onward in *cepr1-3*. For siliques with nonzero fecundity, the average seed set was significantly lower in *cepr1-1* and *cepr1-3* compared with their respective wild-type lines (Fig. 3, E and F). Moreover, the frequency of clearly fertilized and then aborted seeds (i.e. late-aborting seed) was higher in both *cepr1* mutants compared with their respective wild-type lines, and this phenotype was particularly severe in *cepr1-3* (Fig. 3, G and H).
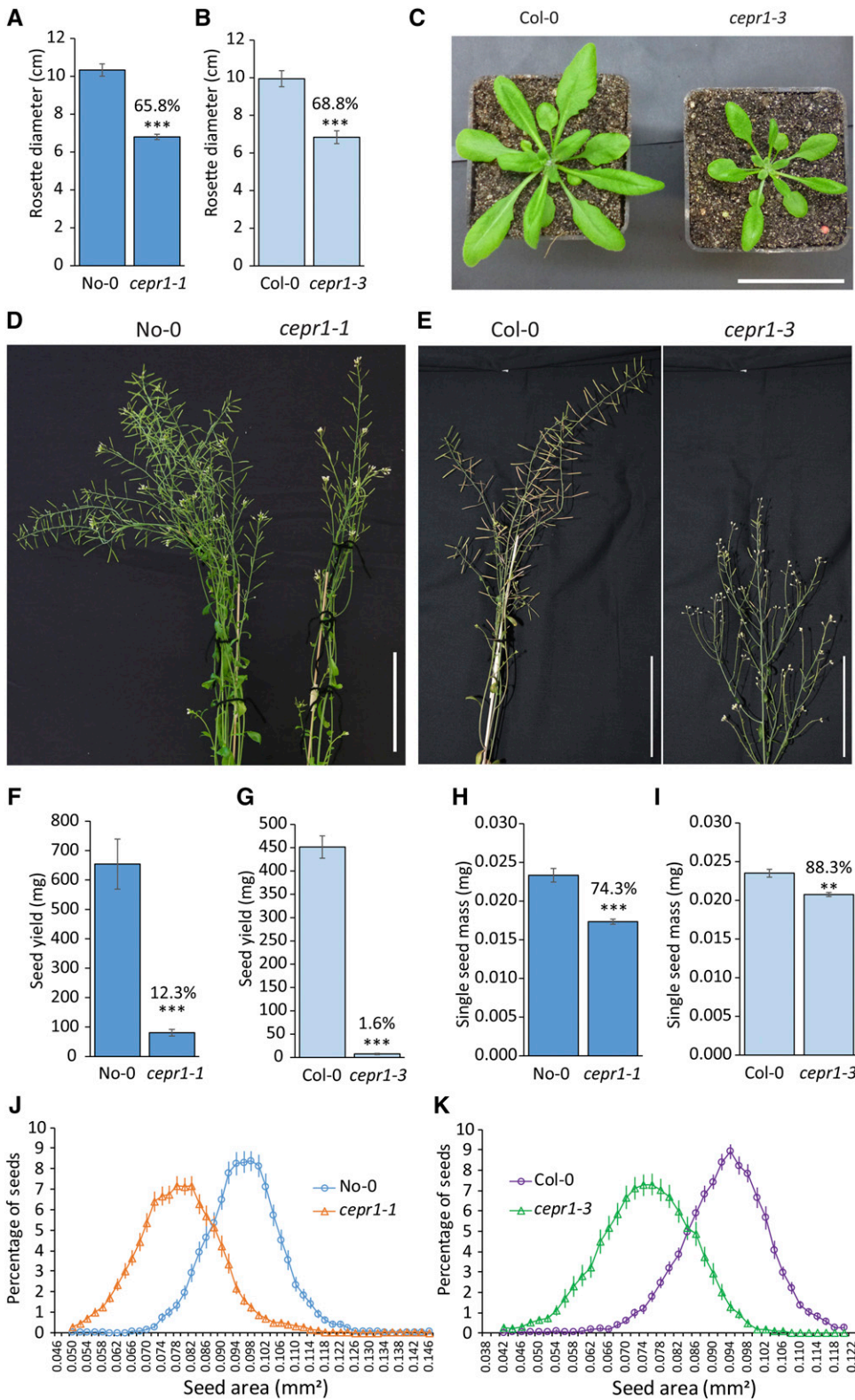
Figure 1. *CEPR1* affects aboveground plant growth, yield, and seed size. A to C, *CEPR1* mutants show decreased vegetative leaf growth. A, Rosette diameter at 30 d post germination (dpg) for No-0 and *cepr1-1*. $n = 10$. B, Rosette diameter at 31 dpg for Col-0 and *cepr1-3*. $n = 4$ to 8. C, Representative images of plants in B. Note that *cepr1-3* rosette leaves displayed no obvious chlorosis. Bar = 5 cm. D to I, Loss of *CEPR1* function results in impaired yield. D, Inflorescence stems of No-0 and *cepr1-1* at 50 dpg. E, Inflorescence stems of Col-0 and *cepr1-3* at 59 dpg. Bars in D and E = 100 mm. F and G, *CEPR1* mutants show reduced yield. Total seed yield per plant is shown for No-0 and *cepr1-1* ($n = 6$–10; F) and for Col-0 and *cepr1-3* ($n = 4$–8; G). H and I, *CEPR1* mutants have reduced seed size. Mass of one seed for No-0 and *cepr1-1* ($n = 3$ plants; H) and for Col-0 and *cepr1-3* lines ($n = 4$ plants; I) was determined from ~100 seeds per plant. Percentages above bars indicate means as a percentage of the wild type. Significant differences were determined by a two-sample Student's t test: **$P <$ 0.01 and ***$P <$ 0.001. Error bars indicate SE. J and K, Distribution of seed size for the wild type and *cepr1* in the No-0 (J) and Col-0 (K) backgrounds. $n = 4$ to 7 plants, 60 to 120 seeds per plant.

Figure 2. CEPR1 affects the development of reproductive organs. Representative images show floral and reproductive organ phenotypes of wild-type and *cepr1* mutant plants in the No-0 and Col-0 accessions. A to D, Inflorescences of the wild type and *cepr1* mutants. The developing buds of *CEPR1* knockout mutants are chlorotic. E to H, Side views of the inflorescences showing chlorotic sepals (sep.) and anthocyanin accumulation in the siliques, pedicle, and main stem of *cepr1* (arrows). The arrowhead in F indicates the fading of anthocyanin in older siliques. I to P, Medial views of dissected wild-type and *cepr1* flowers showing the aberrant floral development associated with *CEPR1* knockout. I to L, Preanthesis stage 12 wild-type and *cepr1* flowers. The arrowhead in L indicates the poorly developed distal end of a *cepr1-3* gynoecium. M and N, Postanthesis stage 13 flowers of wild-type No-0 and *cepr1-1*. O and P, Postanthesis stage 14 flowers of wild-type Col-0 and *cepr1-3*. Bars = 1 mm.


We conducted reciprocal crosses to determine whether the more severe seed set reduction in *cepr1-3* was due to a male and/or female reproductive defect (Fig. 3I). Pollen from *cepr1-3* fertilized wild-type pistils without impairment, which suggested that there was no appreciable decrease in *cepr1-3* pollen viability. The reduced fecundity of the *cepr1-3* pistil compared with the wild type held true regardless of pollen genotype. As mechanical pollination would overcome pollen deposition defects resulting from asynchronous anther-gynoecium development in *cepr1-3* (Fig. 2, O and P), we reasoned that a female reproductive defect limits *cepr1-3* seed set.

To further explore this female fertility defect, we examined fertilization frequency depending on ovule position in the pistil. Such analysis helps distinguish between problems with pollen transmission and ovule-specific defects (Kay et al., 2013; Groszmann et al., 2020). As *cepr1* mutants in both backgrounds had fewer ovules per pistil than the wild type (Supplemental Fig. S2), we assessed seed set at normalized ovule positions within the carpels, from position 0 (closest to the stigma) to position 1 (closest to the gynophore; Fig. 3, J and K). Compared with wild-type No-0, *cepr1-1* showed a

similar, albeit more accentuated, position-dependent fertilization pattern in the pistil (Fig. 3J). As expected, ovules of wild-type Col-0 pistils showed a high and mostly position-neutral fertilization frequency (Fig. 3K). In stark contrast, the fertilization rate in *cepr1-3* was very low at the stigma end and gradually increased toward the proximal region of the pistil, eventually reaching wild-type Col-0 levels (Fig. 3K). The high fertilization rate of ovules farthest from the stigma in *cepr1-3* demonstrates that pollen tubes can traverse the entire distance of the transmitting tract tissue. This indicates that the defect responsible for the reduced ovule fertility is not in the female pollen-transmitting tissues (e.g. stigma and transmitting tract) but rather is specific to the ovules. This fertilization pattern of *cepr1-3* correlated spatially with the poor development of the distal region of the gynoecium (Fig. 2, L and P).

CEPR1 Activity Controls Seed Filling

One component of the yield decrease in *cepr1* is a reduction in mature seeds per silique due to a reduced
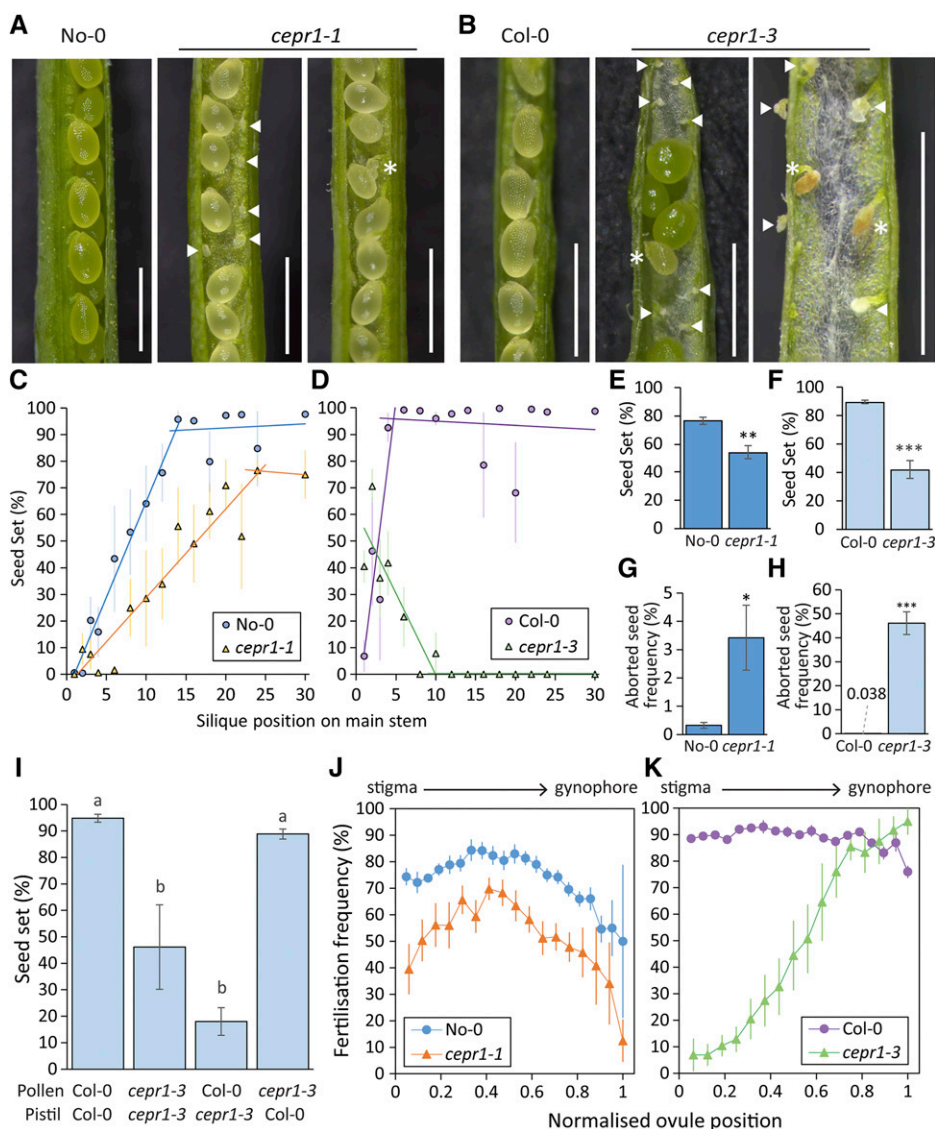
Figure 3. Loss of *CEPR1* function results in decreased seed set and a higher frequency of seed abortion. A and B, Representative images of dissected siliques from self-pollinated wild-type and *cepr1* lines in the No-0 (A) and Col-0 (B) backgrounds. Arrowheads indicate unfertilized ovules. Asterisks indicate aborted seeds. Bars = 1 mm. C and D, Seed set at silique positions on the main stem (position 1 = first silique produced) for self-pollinated wild-type and *cepr1* lines in the No-0 ($n = 4$–6; C) and Col-0 ($n = 3$–6; D) backgrounds. Error bars show SE. For each plant line, two separate linear trend lines were applied to the distinct subset of silique positions before and after a plateau in seed set. E and F, Average seed set determined from siliques with nonzero seed set irrespective of silique position for self-pollinated wild-type and *cepr1* plants in the No-0 background ($n = 6$ plants, seven to 14 siliques per plant; E) and the Col-0 background ($n = 5$–6 plants, two to 15 siliques per plant; F). G and H, Frequency of aborted seeds observed at fertilized ovule positions for self-pollinated wild-type and *cepr1* plants in the No-0 background ($n = 6$ plants, seven to 14 siliques per plant; G) and the Col-0 background ($n = 5$–6 plants, two to 15 siliques per plant; H). Significant differences in E to H were determined by a two-sample Student's t test: $*P < 0.05$; $**P < 0.01$; and $***P < 0.001$. Error bars show SE. I, Percentage seed set for controlled pollination between Col-0 and *cepr1-3* plants. Preanthesis flowers were emasculated prior to deposition of donor pollen onto recipient pistils. Significant differences were determined by ANOVA followed by Tukey's honestly significant difference (HSD) test ($\alpha = 0.05$). $n = 4$ to 6 siliques from three plants. Error bars show SE. J and K, Fertilization frequency at ovule positions for self-pollinated wild-type and *cepr1* plants in the No-0 background ($n = 6$ plants, seven to 14 siliques per plant; J) and the Col-0 background ($n = 5$–6 plants, two to 15 siliques per plant; K). Each position is represented as a fraction of the highest position observed in at least three plants per genotype (0 = stigma end; 1 = gynophore end). Fertilization frequency was determined from siliques with nonzero seed set.

ovule number, a lower fertility rate, and an increased incidence of seed abortion. In addition, *cepr1* seeds that successfully progress to maturity are smaller than wild-type seeds, further contributing to the lower yield. Normally, plants with a reduced seed number tend to compensate by having larger seeds, which is due to a greater proportional allocation of the available nutrients being remobilized from the rosette (Bennett et al., 2012). Therefore, the small mature seeds of *cepr1* may reflect a deficiency in nutrient supply to the seeds. This may arise due to its smaller source rosette and, hence, a proportionately lower per seed availability of nutrients, or alternatively, due to a reduced capacity of *cepr1* plants to deliver nutrients from the source rosette to the seed. To test these possibilities, we manipulated nutrient allocation from the rosette (source) by thinning the number of competing reproductive organs (sinks) to improve the source-to-sink ratio in favor of larger seeds in the siliques that remained (Bennett et al., 2012). As expected, we found that seed size increased in response to the thinning of wild-type plants; however, an increase in seed size did not occur in *cepr1-1* despite improving the source-to-sink ratio (Fig. 4). This result suggests that *CEPR1* is required for the redistribution and/or delivery of resources for seed filling and, in doing so, controls seed size.

CEPR1 Control of Seed Size Depends on *CEPR1* Activity in the Reproductive Bolt

We undertook reciprocal bolt grafting between the wild type and *cepr1-1* to elucidate if CEPR1 activity in the vegetative tissues or reproductive tissues determined seed size (Fig. 5, A and B; Supplemental Fig. S3). Early observations of established grafted bolts revealed that both the chlorosis and the accumulation of anthocyanins in the siliques and inflorescence stem persisted in *cepr1* bolts even when grafted onto wild-type stock (Fig. 5C). This result suggested that juvenile *cepr1* bolts derived little or no additional nutritional benefit from the wild-type stock. At maturity, we harvested the seeds and other dry bolt materials (i.e. stem, cauline leaves, and floral and silique material) to assess the effect of graft combination on seed size and yield. We found that the smaller size of seeds produced by *cepr1* bolts could not be rescued by grafting to a wild-type stock (Fig. 5D). In contrast, there was no penalty to the seed size of wild-type bolts when grafted to *cepr1-1* stock (Fig. 5D). Furthermore, the distribution of seed size for wild-type bolts was more uniform than for *cepr1-1* bolts regardless of the stock (Fig. 5E). This suggests that local CEPR1 activity in the bolt controls seed size and its uniformity. A weak, compensatory effect of vegetative CEPR1 activity was observed for *cepr1-1* bolts grafted onto a wild-type stock (i.e. *cepr1-1*/wild type), with mild improvements in seed size uniformity compared with *cepr1-1* homografts (Fig. 5E).

CEPR1 Activity Controls Total Seed Yield Primarily in the Reproductive Bolt

Since the decrease in total seed yield of the *cepr1-1* bolt could not be rescued by grafting to a wild-type stock (Fig. 6A), a lack of CEPR1 activity in the bolt most likely limits yield in *cepr1-1* plants. Moreover, there was no yield penalty to a wild-type bolt when grafted to a *cepr1* stock but, rather, an apparent increase in total seed yield relative to the wild-type homografts (Fig. 6A). An examination of the dry mass of harvested bolt material (excluding seed) revealed that wild type-on-*cepr1-1* grafts had significantly greater bolt dry mass than the other graft combinations (Fig. 6B), consistent with the greater bolt growth observed for this graft combination at 26 d (Fig. 5B). To account for differences in bolt growth, we calculated the ratio of seed yield to total bolt biomass (bolt harvest index; Fig. 6C). The bolt harvest index of wild type-on-*cepr1-1* grafts was not different from that of wild-type homografts. Compared with the *cepr1-1* homografts, the bolt harvest index of *cepr1-1* slightly improved when grafted to a wild-type stock (increasing from ~37% to ~50% of wild-type homografts). Therefore, while a wild-type stock could
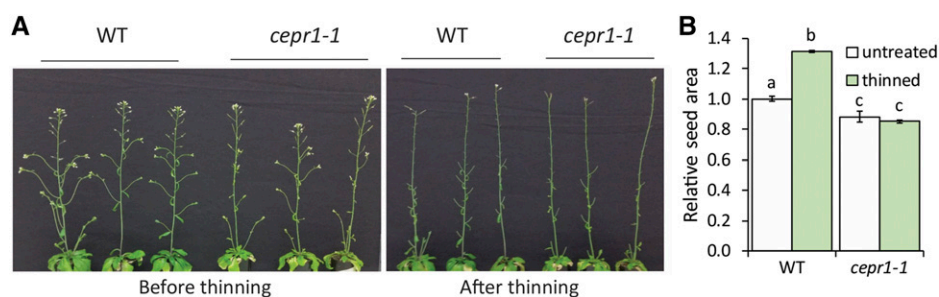
Figure 4. *CEPR1* determines the extent of seed filling. The resource availability per silique was increased by thinning the number of reproductive sinks. A, Images of No-0 (wild type [WT]) and *cepr1-1* before (left) and after (right) thinning. Three to four open flowers or early-stage siliques were left at the apex of the main stem. B, Relative seed area for thinned and untreated plants. Significant differences were determined by ANOVA followed by Tukey's HSD test ($\alpha = 0.05$). $n = 3$ plants, 100 to 200 seeds per plant. Error bars show SE.
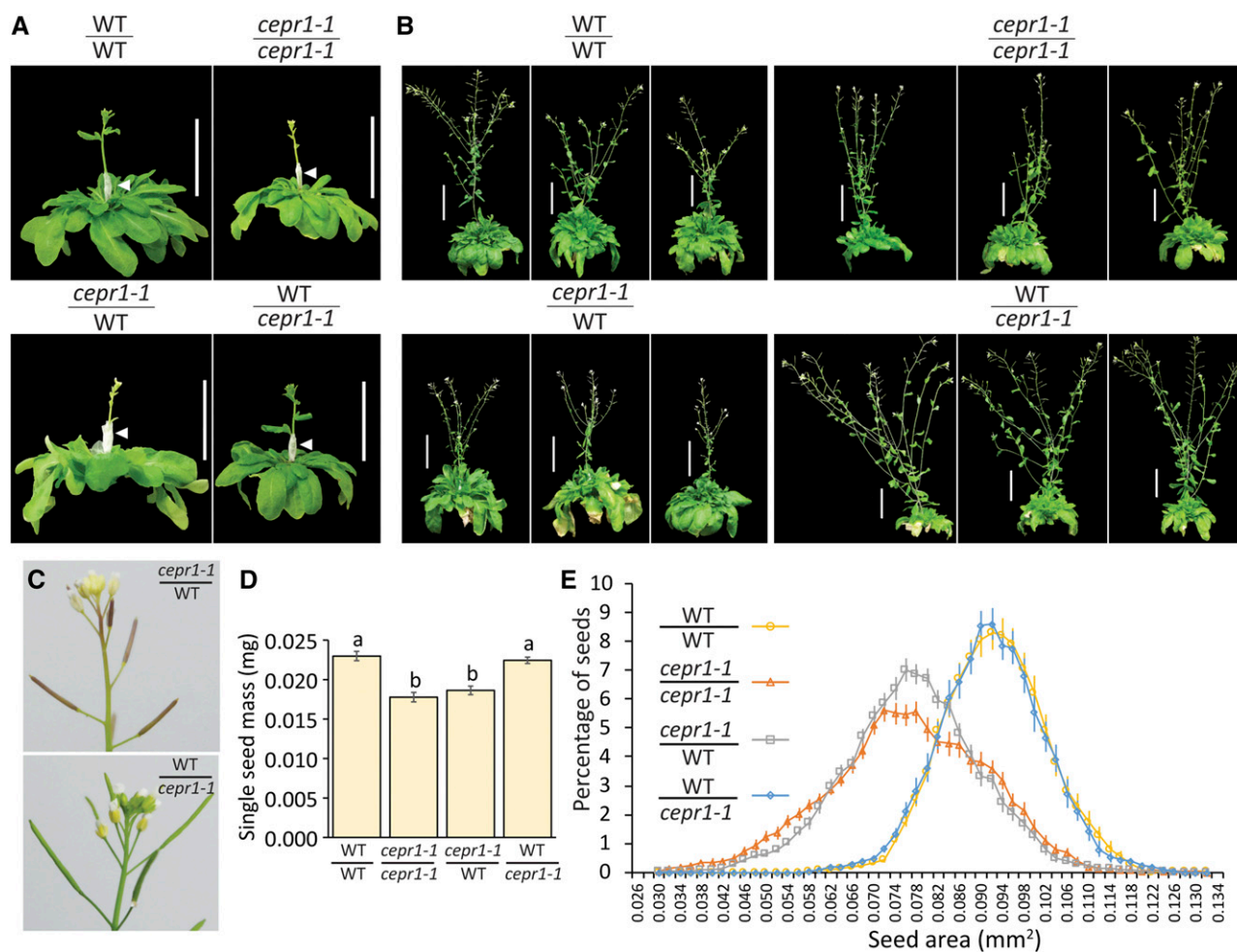
Figure 5. Seed size depends upon *CEPR1* activity in the bolt. Young No-0 (wild-type [WT]) and *cepr1-1* bolts were excised approximately 2 cm from the base and grafted to a recipient stock, which provided vegetative rosette and root tissues to the transplanted reproductive tissue. Secondary branches that formed from the stock after grafting were continuously removed so that the final reproductive organs were derived from the donor bolt only. The bolt and stock genotypes are labeled above and below the horizontal line, respectively. A and B, Reciprocal grafting of wild-type and *cepr1-1* plants. Representative images show plants 0 (A) and 26 (B) d after grafting (bolt/stock genotype). Arrowheads in A indicate the graft junction. Bars = 5 cm. C, Representative images of inflorescences from heterografted plants. Note the accumulation of anthocyanin in the siliques of *cepr1-1* bolt grafts. D, Quantification of single seed mass for grafted plants. Statistically significant differences were determined by ANOVA followed by Tukey's HSD test (α = 0.05). n = 6 to 9. E, Distribution of seed size. n = 6 to 9 plants, 100 to 200 seeds per plant. Error bars show SE.

partially compensate for a lack of CEPR1 in the bolt, the bolt harvest index was primarily determined by CEPR1 activity in the bolt. These results, together with the seed size data, show that CEPR1 bolt activity controls reproductive development, seed size, and subsequently total yield.

CEPR1 Is Expressed in the Vasculature of Floral and Reproductive Organs

To help elucidate how CEPR1 influences reproductive development and fecundity, we examined *CEPR1* expression in reproductive organs using a 2-kb *CEPR1*

promoter-*GUS* reporter (*pCEPR1*:*GUS*). *pCEPR1*:*GUS* was expressed in the vasculature of the inflorescence stem, the base of floral buds, as well as floral and reproductive organs (Fig. 7, A and B). In flowers, expression was detected in the vasculature of well-developed sepals and petals, elongated stamen filaments (Fig. 7, A, C, and D), developing gynoecium prior to fertilization (Fig. 7E), mature gynoecium (Fig. 7F), and the growing silique (Fig. 7G). *CEPR1* expression in the maternal reproductive tissues appeared throughout the entire vasculature network, including the medial and lateral vascular strands, the terminating vascular bundles in the style, and the vasculature of the funiculus right to the point of termination within the chalazal seed coat
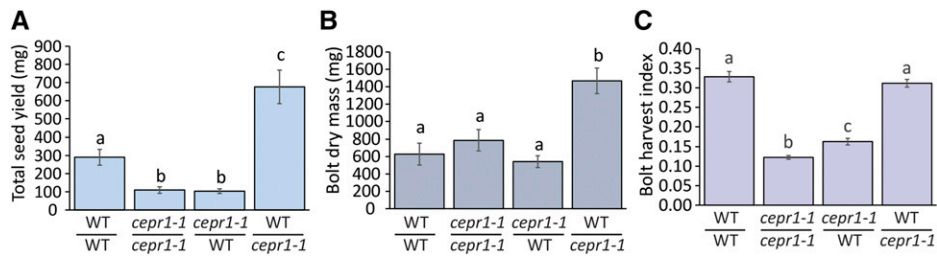
Figure 6. Yield is primarily determined by *CEPR1* activity in the reproductive bolt. Analysis of yield is shown on a per plant basis for reciprocal wild-type (WT) and *cepr1-1* bolt-grafted plants (bolt/stock genotype). Quantification of total seed yield (A), bolt dry mass (minus seed; B), and bolt harvest index (the ratio of seed yield to total bolt biomass; C) are shown. Significant differences were determined by ANOVA followed by Tukey's HSD test ($\alpha = 0.05$). Error bars show SE. $n = 6$ to 9 plants.

(Fig. 7, F–H). We observed *CEPR1* expression within the funiculus and chalazal seed coat only after fertilization (Fig. 7, E and F), and it persisted throughout seed development (Fig. 7, H and I). We detected no expression of *CEPR1* in the endosperm or embryo.

The restriction of seed *pCEPR1:GUS* expression to the chalazal seed coat is consistent with publicly available expression data (Fig. 7J; Belmonte et al., 2013; Arabidopsis eFP browser [https://bar.utoronto.ca/efp/cgi-bin/efpWeb.cgi]). *CEPR1* expression in the chalazal seed coat is important since it represents the final delivery point of nutrients via the vasculature from the mother tissue prior to their uptake via a variety of transporters to the symplasmically isolated filial tissues (Stadler et al., 2005; Chen et al., 2015; Müller et al., 2015; Hoai et al., 2020). The lack of *pCEPR1:GUS* or *CEPR1* mRNA expression in the endosperm or embryo tissue indicates that *CEPR1* control of seed size occurs strictly through activity in the mother tissue. Consistent with this, restoring wild-type *CEPR1* in only the filial tissue of the *cepr1-3* mutant via crossing (i.e. *cepr1-3* ♀ × wild-type Col-0 ♂) did not improve seed size (Supplemental Fig. S4).

Transgenic *CEPR1* Rescues *cepr1* Reproductive and Yield Defects

We complemented both *cepr1* mutants using a transgene containing *CEPR1* driven by the same 2-kb upstream sequence used in our GUS reporter expression analysis (Fig. 8). The examination of multiple complemented lines revealed that the transgene rescued several obvious *cepr1* developmental defects (e.g. anthocyanin accumulation in stem and silique, smaller chlorotic flowers, and aberrant floral organ morphology; Fig. 8, A and B). Further analysis of two independent complemented lines of each *cepr1* allele demonstrated full or substantial rescue of ovule number (Fig. 8, C and G), seed set (Fig. 8, D and H), seed abortion (Fig. 8, E and I), and seed size (Fig. 8, F and J). These results indicate that the 2 kb of sequence upstream of *CEPR1* is sufficient for native *CEPR1* function and imply that a loss of *CEPR1* expression in the vasculature is the causal factor leading to the developmental, reproductive, and yield defects associated with the *cepr1* mutants.

CEPR1 Regulates the Expression of Genes Involved in Nitrogen Homeostasis in the Reproductive Bolt

Anthocyanin accumulation and chlorosis are signs of imbalances in nitrogen and carbon, especially where nitrogen is low and carbon is in proportional excess (Takatani et al., 2014). Therefore, nutritional limitation may account for the *cepr1* defects in floral morphology, lower fecundity, high incidence of seed abortion, and smaller, more variable seed sizes. To investigate this, we harvested bolt and inflorescence tissues and surveyed the expression of several genes involved in the CEP-CEPR1 signaling pathway along with several genes involved in nitrogen and carbon homeostasis (Fig. 9). *CEPD1*, which is positively regulated by CEP-CEPR1 signaling in shoots (Ohkubo et al., 2017), was down-regulated approximately 8-fold in the *cepr1* bolt tissue (Fig. 9A). Three out of four CEP ligand-encoding genes known to be expressed in the bolt (Roberts et al., 2013; Col-0 accession) were also differentially expressed in the *cepr1* mutants. *CEP5* and *CEP9* were strongly up-regulated (~32-fold), *CEP2* was down-regulated in *cepr1-3* (approximately 3-fold) and undetectable in the No-0 background, and *CEP1* expression was not significantly altered (Fig. 9A). The *cepr1* mutants had an ~60% reduction in the expression of *GLUTAMINE SYNTHETASE1;2* (*GLN1;2*; Fig. 9B), which encodes the main isozyme contributing to Gln synthetase activity in the shoot (Guan et al., 2016) and is known to be involved in nitrogen mobilization and yield formation (Diaz et al., 2008; Guan et al., 2016; Moison et al., 2018). The expression of the nitrate reductase gene *NITRATE REDUCTASE1* (*NIA1*), also involved in nitrogen metabolism (Wilkinson and Crawford, 1993), was not significantly different. The expression of *UMAMIT14*, an amino acid transporter gene linked to seed filling (Müller et al., 2015), was strongly down-regulated in the *cepr1* mutants (greater than 80% reduction; Fig. 9B). In contrast, *UMAMIT11* and *UMAMIT18/SILIQUES ARE RED1* (*SIAR1*), which also supply assimilated nitrogen as amino acids to reproductive tissues (Ladwig et al., 2012; Müller et al., 2015), were not
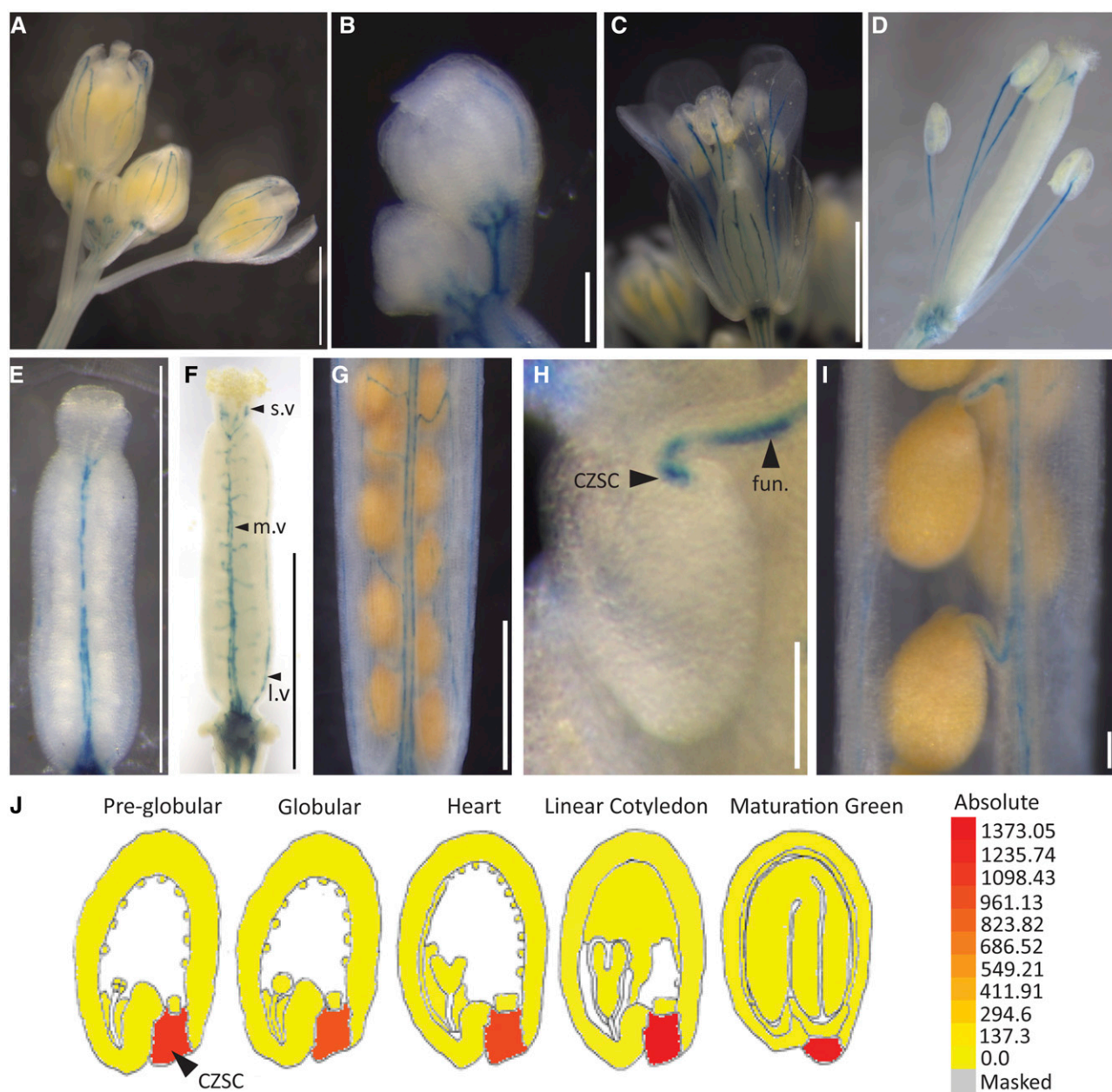
Figure 7. *CEPR1* expresses in the vasculature of reproductive organs. A to I, *pCEPR1:GUS* expression in the reproductive organs. Shown are whole inflorescence (A), buds (B), stage 14 flower (C), stage 15 gynoecium and stamens (D), stage 12 gynoecium (E), stage 14 gynoecium (F; l.v, lateral vasculature; m.v, medial vasculature; s.v, style vasculature; mature silique (G), funiculus (fun.) and chalazal seed coat (CZSC; H), and mature silique funiculus (I). Staining was carried out for 18 h (A, D, G, and I), 24 h (H), or 72 h (B, C, E, and F). Bars = 1 mm (A and C–G) and 0.1 mm (B, H, and I). J, Microarray expression of *CEPR1* in the developing seed from the Arabidopsis eFP browser (https://bar.utoronto.ca/efp/cgi-bin/efpWeb.cgi; Belmonte et al., 2013).

differentially expressed in the *cepr1* mutants (Fig. 9B). Consistent with the observed anthocyanin accumulation in *cepr1* stems, there was a substantial up-regulation in the *cepr1* mutants of one or both of the low-nitrogen-induced MYB transcription factors *PRODUCTION OF ANTHOCYANIN PIGMENT1* (*PAP1*) and *PAP2*, which are involved in anthocyanin production when nitrogen is limited (Scheible et al., 2004; Lea et al., 2007; Rubin et al., 2009; Fig. 9B).

Unlike some of the nitrogen-associated genes, marker genes responding to elevated carbon (Nunes et al., 2013; Cookson et al., 2016) were not substantially altered in the *cepr1* mutants. Specifically, *AKINBETA1* and the putative trehalose-6-phosphate synthase genes, *TREHALOSE PHOSPHATE SYNTHASE8* (*TPS8*) and *TPS10*, which are normally down-regulated in response to elevated carbon levels, were either mildly down-regulated or unaltered in the *cepr1* mutants (Fig. 9C).
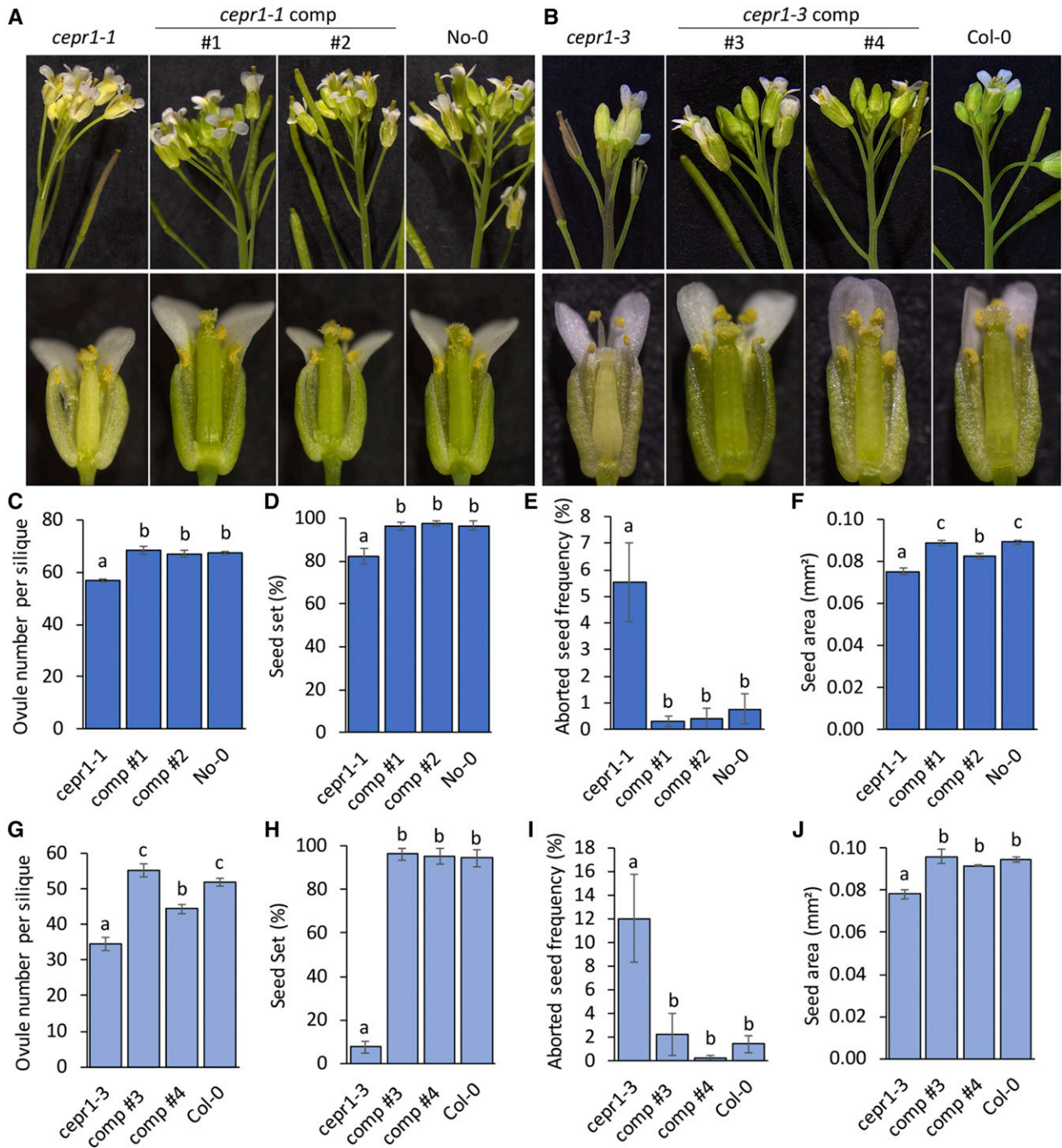
Figure 8. Complementation of *cepr1* mutants using a *CEPR1* genomic fragment. Reproductive development phenotypes were assessed for independent complementation (comp) lines in the No-0 *cepr1-1* (1 and 2) and Col-0 *cepr1-3* (3 and 4) backgrounds compared with their respective *cepr1* mutant and wild-type lines. A and B, Representative images showing side views of the inflorescence (top row) and dissected postanthesis flowers (bottom row) for lines in the No-0 (A) and Col-0 (B) ecotypes. C and G, Quantification of ovule number for siliques with nonzero fecundity for No-0 (n = 4–10, two siliques per plant; C) and Col-0 (n = 3–11, one to four siliques per plant; G) ecotype lines. D and H, Measurement of seed set for No-0 (n = 4–10; D) and Col-0 (n = 3–11; H) ecotype lines. Two siliques were examined per plant from positions on the stem corresponding to the phase of wild-type maximal seed set (Fig. 3, C and D). E and I, Frequency of aborted seeds observed at fertilized ovule positions for lines in the No-0 (n = 4–10, two siliques per plant; E), and Col-0 (n = 3–11, one to four siliques per plant; I) ecotypes. F and J, Seed area for No-0 (n = 6–11 plants; F) and Col-0 (n = 3–9 plants; J) ecotype lines determined from 60 to 120 seeds per plant. Significant differences were determined by ANOVA followed by Fisher's LSD test (α = 0.05). Error bars show SE.
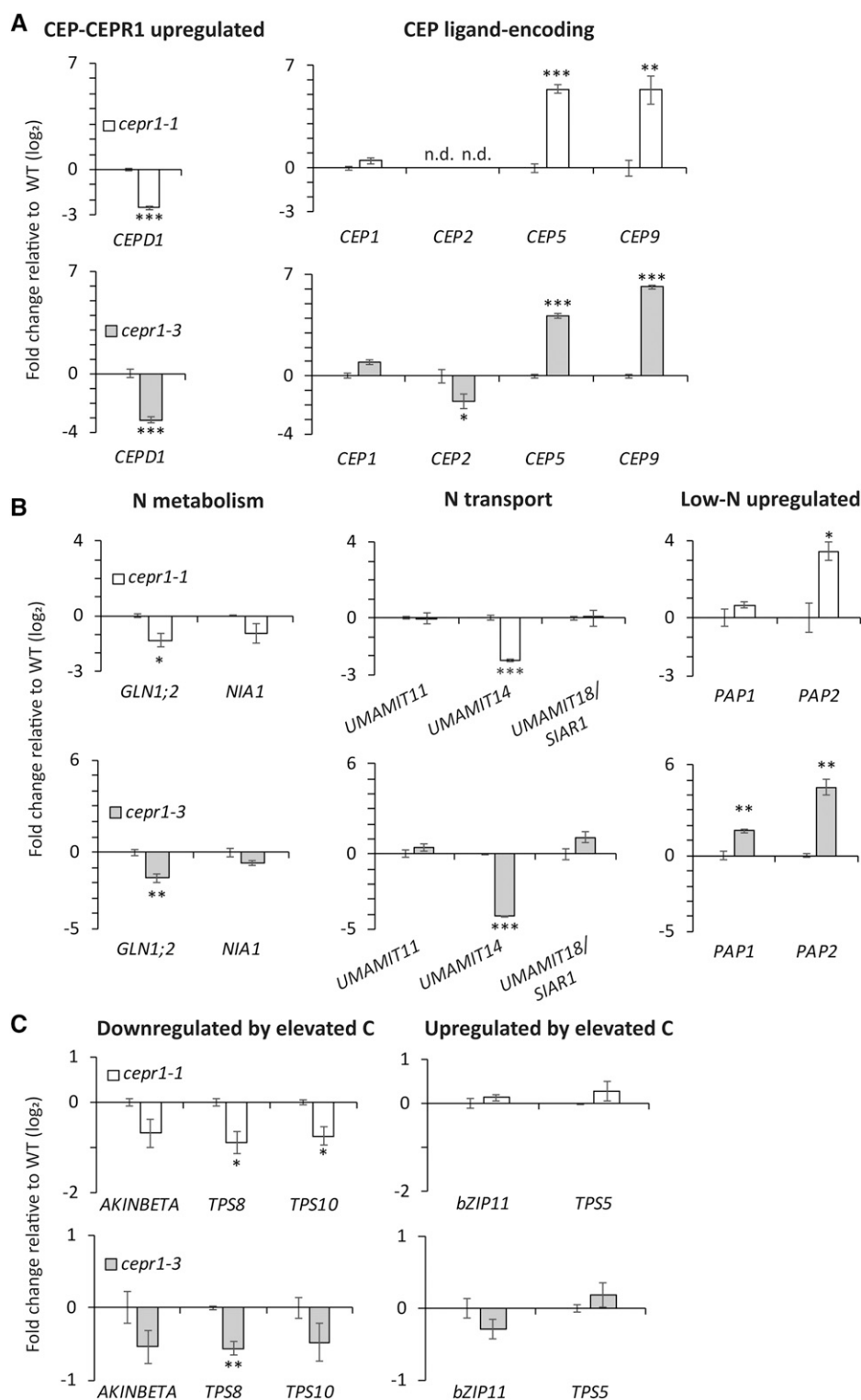
Figure 9. Loss of *CEPR1* function affects the expression of genes involved in nitrogen homeostasis in bolt tissue. For reverse transcription quantitative PCR (RT-qPCR) analyses, the primary inflorescence tissue was harvested from wild-type and *cepr1* plants upon first flower opening. The fold change in expression (log$_2$) was determined for *cepr1-1* and *cepr1-3* relative to the wild-type (WT; No-0 and Col-0, respectively) for a selection of CEP-CEPR1 pathway genes (A), genes related to nitrogen (N) homeostasis (B), and genes related to carbon (C) homeostasis (C). Significant differences were determined by a two-sample Student's *t* test: *$P <$ 0.05; **$P <$ 0.01; and ***$P <$ 0.001. Error bars show SE. $n = 3$ biological replicates each consisting of two pooled plants. n.d., Not detected.

The Arabidopsis *BASIC LEUCINE-ZIPPER11* (*bZIP11*) and *TPS5* genes, which positively respond to elevated carbon levels, remained unchanged (Fig. 9C). Together with the nitrogen-associated transcripts, the expression profiles of *cepr1* bolts imply a state of nitrogen limitation with minimal or no perturbations to carbon status.

DISCUSSION

In this study, we demonstrated a function for CEPR1 in controlling seed yield via a local circuit in the reproductive tissues of Arabidopsis. The severely decreased yield of *cepr1* mutants is due to a loss of vasculature-expressed *CEPR1*, which compromises bolt growth,

female reproductive development, seed set, and mature seed size and, in addition, causes chlorosis and anthocyanin accumulation in inflorescence tissues. The complementation of *cepr1* mutants using a *CEPR1* genomic fragment rescues these diverse phenotypes. Underpinning these phenotypes of the *cepr1* mutants is the apparent common theme of an inability to mobilize nutrients, specifically nitrogen, either from the vegetative tissues to the young bolts or from within bolt tissues to the developing floral organs and seeds. Several lines of evidence support this view.

First, the *cepr1* reproductive tissues showed chlorosis in the bolt tissues and floral organs and anthocyanin accumulation in the inflorescence stems and siliques. The grafting of young *cepr1* bolts onto wild-type vegetative stocks did not remedy these well-documented phenotypes of nutrient limitation stress, suggesting a compromise of nutrient delivery from the vegetative tissue to the young *cepr1* bolt. Concordantly, young wild-type bolts did not develop chlorosis or accumulate anthocyanins when grafted onto *cepr1* vegetative stocks.

The grafting of *cepr1* bolts onto wild-type vegetative stocks did not restore yield or a normal seed size distribution, whereas wild-type bolts had no reduction in yield or seed size when grafted to *cepr1* vegetative stocks. In agreement with a role for *CEPR1* in seed filling through the control of nitrogen mobilization and delivery, we found that both *GLN1;2* and *UMAMIT14* were down-regulated in the *cepr1* reproductive bolt. The cytosolic Gln synthetase encoded by the vasculature-expressed *GLN1;2* contributes to nitrogen remobilization from source tissues for seed filling (Moison et al., 2018), with *gln1;2* loss-of-function mutants displaying reduced seed size and yield similar to *cepr1* (Guan et al., 2015). The importance of cytosolic Gln synthetase in seed filling appears conserved across diverse species, including maize (*Zea mays*; Martin et al., 2006). The *UMAMIT14* amino acid transporter is also expressed throughout the plant vasculature, including the chalazal seed coat, where it is required for the unloading of amino acids transported from source tissues to support seed filling. Consistent with the decreased *UMAMIT14* expression in the *cepr1* mutants, the *umamit14* null mutants produce smaller seeds (Müller et al., 2015).

Improving nutrient allocation by thinning the number of reproductive units resulted in the expected increased seed size in wild-type plants but not in *cepr1* mutants. The differential effect of thinning between the wild type and *cepr1* is not due to the smaller *cepr1* rosettes, because grafting showed that the *cepr1* rosettes support the flourishing of wild-type bolts. Moreover, this grafting result implies that the *cepr1* source rosettes are still able to sufficiently load nutrients such as amino acids into the phloem for export to the developing bolts (Santiago and Tegeder, 2016). Therefore, the seeds of *cepr1* plants that were thinned appear unable to receive the expected allocation of surplus nutrient that clearly benefits the seeds of thinned wild-type plants.

CEPR1 expression was detected throughout the vasculature of reproductive tissues, consistent with a function in nutrient mobilization/delivery. The specific expression of *CEPR1* in the chalazal seed coat, but not in any other seed tissues, is pertinent to the *cepr1* seed size defect, since this tissue is the final delivery point of nutrients from the mother tissue via the vasculature prior to their uptake via transporters to the symplasmically isolated filial tissues (Müller et al., 2015). This localization points to CEPR1 playing an important role in nutrient unloading at the seed and indicates that it controls seed development and size strictly through activity in the maternal tissue. An impairment of nutrient delivery to the seed would be consistent with the more variable seed size and higher rates of seed abortion observed in the *cepr1* mutants, with seed abortion occurring in instances where early nutrient demands of the embryo are not met (Di Berardino et al., 2018) and with the more variable mature seed sizes reflecting inconsistency in nutrient delivery.

Our RT-qPCR data indicate that the nutrient stress caused by a loss of *CEPR1* function is related to impaired nitrogen status of the reproductive bolt. Consistent with a low nitrogen state and anthocyanin accumulation, *cepr1* bolts displayed a strong upregulation of one or both of the MYB transcription factors *PAP1* and *PAP2*. These *PAP* genes are highly upregulated in response to nitrogen starvation and positively regulate anthocyanin biosynthesis (Lea et al., 2007; Rubin et al., 2009). The down-regulation of the Gln synthetase gene *GLN1;2* and *UMAMIT14* would be consistent with decreased levels of assimilated nitrogen compounds (Patterson et al., 2010; Besnard et al., 2016). By contrast, the mild down-regulation of carbon-repressed TPS genes and the unchanged expression of carbon-induced transcripts in *cepr1* bolts imply a sufficient carbon supply. A decreased nitrogen state but steady carbon state in *cepr1* mutants is further supported by their accumulation of anthocyanins, which in general is not just a symptom of nitrogen limitation but rather a symptom of excess levels of carbon relative to nitrogen (Takatani et al., 2014). Moreover, several CEP-CEPR1 pathway genes both upstream (i.e. several *CEP* genes) and downstream (i.e. *CEPD1*) of *CEPR1* displayed altered expression in *cepr1* bolts, consistent with a locally perturbed CEPR1 signaling status involving both feedforward and feedback loops. Similar transcriptional perturbations occur to CEP-CEPR1 pathway genes locally in *cepr1* root tissues (Chapman et al., 2019). These transcriptional responses, together with *CEPR1* expression in the vasculature of reproductive tissues and the dependence of seed size and yield on local CEPR1 activity, demonstrate that CEPR1 specifically acts in bolt tissues to control aspects of nitrogen mobilization and delivery to reproductive sinks.

Finally, an impairment in the nitrogen economy of the bolt can also explain the *cepr1* fecundity and silique defects. Nutrient deficiency is consistent with the diminished growth of the bolt and the reduced number of reproductive units produced (i.e. flowers and siliques;

Perchlik and Tegeder, 2018). The aberrant and asynchronous development of the *cepr1* gynoecium and stamens, contributing to the reduced seed number on a per silique basis, is comparable with the miscoordination of reproductive development occurring in rice florets when nitrogen is limited by loss-of-function mutations in arginase (OsARG) or ornithine δ-aminotransferase (OsOAT; Ma et al., 2013; Liu et al., 2018). Similar to *cepr1*, these rice mutants display reduced seed set and smaller seed/grain. The accumulation of anthocyanins observed in *cepr1* developing siliques is identical to the phenotype of mutants in the amino acid transporter gene *UMAMIT18/SIAR1* and is likely a stress symptom of inadequate nitrogen provision during the nutrient-demanding stages of seed development (Ladwig et al., 2012). The miscoordination of reproductive development along with the altered expression of some nitrogen-related genes in the *cepr1* bolt are consistent with *CEPR1* acting as one node of a complex network regulating nitrogen homeostasis (Castaings et al., 2011; Tegeder and Masclaux-Daubresse, 2018).

CONCLUSION

In this article, we show that CEPR1 activity in the reproductive tissue is critical for both reproductive development and yield. Our data highlight the importance of CEPR1 activity in the reproductive bolt for the delivery of nutrients for yield formation. The apparent perturbation of nitrogen status in *cepr1* bolts suggests that CEPR1 plays a broader role in controlling nitrogen homeostasis at the whole-plant level beyond roles previously identified in root nitrogen acquisition, root system architecture, and nodulation (Huault et al., 2014; Tabata et al., 2014; Mohd-Radzman et al., 2016; Ohkubo et al., 2017; Chapman et al., 2020). The manipulation of CEPR1-dependent outputs could provide a new avenue to improve nutrient delivery from source tissues to reproductive sinks, with the aim of improving traits such as seed yield and nitrogen use efficiency in plants.

MATERIALS AND METHODS

Plant Materials and Growth Conditions

The previously described Arabidopsis (*Arabidopsis thaliana*) No-0 *cepr1-1* (RATM11-2459 [RIKEN]; Bryan et al., 2012; Tabata et al., 2014) and Col-0 *cepr1-3* (467C01 [GABI-Kat]; Kleinboelting et al., 2012; Chapman et al., 2019) mutant lines were used. Sterilized seedlings were grown on solidified medium (1% [w/v] type M agar) containing one-half-strength Murashige and Skoog basal salts (Sigma) at pH 5.7 for 7 to 10 d until seedlings were transferred to soil (seed-raising mix; Debco) supplemented with Osmocote Exact fertilizer and grown in chambers at 22°C. For the grafting experiment, plants were grown with 200 μmol m^{-2} s^{-1} light and an 8-h photoperiod. For all other experiments, plants were grown with 100 μmol m^{-2} s^{-1} light and a 16-h photoperiod.

Determination of Seed Size, Seed Set, and Yield Parameters

Inflorescences were covered with microperforated plastic bags to collect seeds. To determine single seed mass, aliquots were weighed and seed number

per aliquot was counted. Seed area was determined using ImageJ (https://imagej.nih.gov/ij/) using the particle analysis function with a consistently applied threshold on all microscope images of seeds taken with identical magnification and exposure time within experiments (Herridge et al., 2011). For seed size distributions, the percentage of seeds within bins at 0.002-mm^2 intervals was determined and a running average over six bins was plotted. For controlled pollination, preanthesis flowers (Smyth et al., 1990; stage 12) were emasculated using forceps. One day after emasculation, the pollen from the donor genotype was applied to the stigma of the recipient genotype. Seed development and seed set were determined by dissecting developing siliques and dehisced siliques, respectively (Groszmann et al., 2008; Kay et al., 2013). For the grafting experiment, the bolt harvest index was determined as the seed mass as a proportion of total bolt biomass (seed mass/total bolt dry mass including seed).

Vector Construction

To generate the *pCEPR1:GUS* reporter, the 2 kb of sequence upstream of the start codon of *CEPR1* was amplified from Col-0 gDNA, cloned into pENTR/D-TOPO, and then transferred into the pHGWFS7 destination vector (Karimi et al., 2002) by LR recombination. To generate the *CEPR1* complementation construct, the kanamycin marker for plant selection in the pBI121 vector was first removed by digestion with *Pme*I and *Apa*I and was replaced using Gibson Assembly (New England Biolabs) with a Basta selection marker amplified from the MIGS2.1 vector (de Felippes et al., 2012). Using Gibson Assembly, the Col-0 *CEPR1* genomic fragment and 2 kb of upstream sequence was cloned upstream of a *NOS* terminator in the modified pBI121 vector cut with *Sac*I and *Cla*I. Primer sequences used for cloning are listed in Supplemental Table S1.

Plant Transformation and Introgression of Constructs

Plants were transformed by floral dipping (Clough and Bent, 1998) with the *Agrobacterium tumefaciens* strain LBA4404 harboring the described vectors to create the *pCEPR1:GUS* reporter line (No-0 background) and the *cepr1-1* complementation lines (comp 1 and comp 2). Due to the severely impaired female fertility in *cepr1-3*, which prevented the direct transformation of this mutant, the complementation lines in the *cepr1-3* background (comp 3 and comp 4) were generated by crossing with wild-type Col-0 transformed with the complementation construct. Flowers from independent Col-0 lines harboring the *CEPR1* complementation construct were emasculated and then pollinated using *cepr1-3* pollen. F2 plants homozygous for the *cepr1-3* allele (i.e. no endogenous wild-type *CEPR1*) and carrying the *CEPR1* transgene were identified using PCR genotyping (for primers, see Supplemental Table S1).

Thinning Experiment

Six-week-old No-0 (wild-type) and *cepr1-1* plants were thinned by removal of siliques and flowers in addition to secondary and lateral apexes so that only three or four open flowers or very-early-stage siliques remained on the primary stem. Seeds from thinned plants were compared with those from unpruned controls.

Inflorescence Stem (Bolt) Grafting

Bolt grafting was carried out as described by Nisar et al. (2012). Briefly, young No-0 (wild-type) and *cepr1-1* bolts (~80 mm long) were excised ~20 mm from the base. The end of the donor bolt was cut into a wedge, which was inserted into a vertical incision made in the remaining basal stem section of the recipient stock. The graft junction was stabilized with silicon tubing of 2 to 2.5 mm (internal diameter) and covered with Parafilm to retain moisture. Plants were kept in a humid environment using a plastic covering until grafted bolts had reestablished turgor and growth. Bolts that did not take, or that grew poorly as determined by the appearance of necrotic cauline leaves, were discarded. Secondary branches that formed from the stock after grafting were continuously removed so that the final reproductive organs were derived from the donor bolt only.

Promoter-GUS Reporter Analysis

GUS staining and analysis were performed essentially as previously described (Groszmann et al., 2010, 2011). Briefly, samples were harvested into cold

phosphate buffer (pH 7) with 4% (v/v) formaldehyde, washed in cold phosphate buffer, transferred into 2 mM 5-bromo-4-chloro-3-indolyl-β-D-glucuronic acid staining solution, incubated at 37°C for specified durations, and then cleared for 24 h in 70% (v/v) ethanol, fixed for 24 h in 70% (v/v) ethanol plus FAA (3.7% [v/v] formaldehyde and 5% [v/v] acetic acid), washed again, and stored in 70% (v/v) ethanol ready for visualization.

Microscopy

Microscopic imaging was carried out with an M205 FA stereomicroscope with a DFC550 camera (Leica).

Complementation Analyses

T2 complementation lines in the *cepr1-1* background (comp 1 and comp 2) were grown alongside wild-type No-0 and *cepr1-1*. PCR genotyping identified *cepr1-1* plants harboring the complementation transgene and null (azygous) segregants. Azygous segregants were pooled with the *cepr1-1* plants grown in parallel for the analysis.

For complementation lines in the *cepr1-3* background (comp 3 and comp 4), segregating F2 plants were grown alongside wild-type Col-0 and *cepr1-3*. PCR genotyping identified homozygous *cepr1-3* plants harboring the complementation *CEPR1* transgene. For the analysis, wild-type Col-0 and *cepr1-3* segregants identified from the F2 populations were pooled with the wild-type Col-0 and *cepr1-3* plants grown in parallel, respectively. See Supplemental Table S1 for genotyping primers used.

RT-qPCR Analyses

Wild-type and *cepr1* primary inflorescence tissue (including stem, inflorescence meristem, buds, and flowers) was harvested for analyses upon opening of the first flower. The lateral organs (cauline leaves, developing branches, and buds) were removed from the harvested tissue before they were snap frozen in liquid nitrogen. Three biological samples per genotype, each containing two bolts, were used, and total RNA was isolated by a modified Trizol extraction method using columns from the RNeasy Plant Mini Kit (Qiagen; Delay et al., 2013b). cDNA synthesis was carried out using oligo(dT)$_{12-18}$ primers and SuperScript III reverse transcriptase (Invitrogen) and was followed by treatment with RNase H (Invitrogen). For RT-qPCR, Fast SYBR Green fluorescent dye (Applied Biosystems) was used, and samples were run on a ViiA 7 Real-Time PCR System (Applied Biosystems) following the manufacturer's specifications. Data were analyzed using the $\Delta\Delta C_T$ method (Livak and Schmittgen, 2001), with *EF1α* (At1g07920) expression used for normalization (Czechowski et al., 2005). RT-qPCR primers are listed in Supplemental Table S1.

Accession Numbers

The Arabidopsis Genome Initiative locus codes for the genes discussed in this study are as follows: *CEPR1* (AT5G49660), *CEPD1* (AT1G06830), *CEPD2* (AT2G47880), *CEP1* (AT1G47485), *CEP2* (AT1G59835), *CEP5* (AT5G66815), *CEP9* (AT3G50610), *UMAMIT11* (AT2G40900), *UMAMIT14* (AT2G39510), *UMAMIT18/SIAR1* (AT1G44800), *PAP1* (AT1G56650), *PAP2* (AT1G66390), *NIA1* (AT1G77760), *GLN1;2* (AT1G66200), *AKINBETA1* (AT5G21170), *TPS5* (AT4G17770), *TPS8* (AT1G70290), *TPS10* (AT1G60140), and *bZIP11* (AT4G34590).

Supplemental Data

The following supplemental materials are available.

Supplemental Figure S1. *CEPR1* mutants have reduced reproductive units per main stem.

Supplemental Figure S2. *CEPR1* knockout results in a reduced number of ovules per silique

Supplemental Figure S3. Rosette diameter of plants grown under a short-day (8-h) photoperiod for bolt grafting.

Supplemental Figure S4. *CEPR1* controls seed size via activity in the maternal tissue.

Supplemental Table S1. List of oligonucleotides used.

LITERATURE CITED

Belmonte MF, Kirkbride RC, Stone SL, Pelletier JM, Bui AQ, Yeung EC, Hashimoto M, Fei J, Harada CM, Munoz MD, et al (2013) Comprehensive developmental profiles of gene activity in regions and subregions of the Arabidopsis seed. Proc Natl Acad Sci USA **110:** E435–E444

Bennett E, Roberts JA, Wagstaff C (2012) Manipulating resource allocation in plants. J Exp Bot **63:** 3391–3400

Besnard J, Pratelli R, Zhao C, Sonawala U, Collakova E, Pilot G, Okumoto S (2016) UMAMIT14 is an amino acid exporter involved in phloem unloading in Arabidopsis roots. J Exp Bot **67:** 6385–6397

Bryan AC, Obaidi A, Wierzba M, Tax FE (2012) XYLEM INTERMIXED WITH PHLOEM1, a leucine-rich repeat receptor-like kinase required for stem growth and vascular development in Arabidopsis thaliana. Planta **235:** 111–122

Castaings L, Marchive C, Meyer C, Krapp A (2011) Nitrogen signalling in Arabidopsis: How to obtain insights into a complex signalling network. J Exp Bot **62:** 1391–1397

Chapman K, Ivanovici A, Taleski M, Sturrock CJ, Ng JLP, Mohd-Radzman NA, Frugier F, Bennett MJ, Mathesius U, Djordjevic MA (2020) CEP receptor signalling controls root system architecture in Arabidopsis and Medicago. New Phytol **226:** 1809–1821

Chapman K, Taleski M, Ogilvie HA, Imin N, Djordjevic MA (2019) CEP-CEPR1 signalling inhibits the sucrose-dependent enhancement of lateral root growth. J Exp Bot **70:** 3955–3967

Chen LQ, Lin IW, Qu XQ, Sosso D, McFarlane HE, Londoño A, Samuels AL, Frommer WB (2015) A cascade of sequentially expressed sucrose transporters in the seed coat and endosperm provides nutrition for the Arabidopsis embryo. Plant Cell **27:** 607–619

Clough SJ, Bent AF (1998) Floral dip: A simplified method for Agrobacterium-mediated transformation of Arabidopsis thaliana. Plant J **16:** 735–743

Cookson SJ, Yadav UP, Klie S, Morcuende R, Usadel B, Lunn JE, Stitt M (2016) Temporal kinetics of the transcriptional response to carbon depletion and sucrose readdition in Arabidopsis seedlings. Plant Cell Environ **39:** 768–786

Czechowski T, Stitt M, Altmann T, Udvardi MK, Scheible WR (2005) Genome-wide identification and testing of superior reference genes for transcript normalization in Arabidopsis. Plant Physiol **139:** 5–17

Czyzewicz N, Yue K, Beeckman T, De Smet I (2013) Message in a bottle: Small signalling peptide outputs during growth and development. J Exp Bot **64:** 5281–5296

de Felippes FF, Wang JW, Weigel D (2012) MIGS: miRNA-induced gene silencing. Plant J **70:** 541–547

Delay C, Chapman K, Taleski M, Wang Y, Tyagi S, Xiong Y, Imin N, Djordjevic MA (2019) CEP3 levels affect starvation-related growth responses of the primary root. J Exp Bot **70:** 4763–4774

Delay C, Imin N, Djordjevic MA (2013a) Regulation of Arabidopsis root development by small signaling peptides. Front Plant Sci **4:** 352

Delay C, Imin N, Djordjevic MA (2013b) CEP genes regulate root and shoot development in response to environmental cues and are specific to seed plants. J Exp Bot **64:** 5383–5394

Diaz C, Lemaître T, Christ A, Azzopardi M, Kato Y, Sato F, Morot-Gaudry JF, Le Dily F, Masclaux-Daubresse C (2008) Nitrogen recycling and remobilization are differentially controlled by leaf senescence and development stage in Arabidopsis under low nitrogen nutrition. Plant Physiol **147:** 1437–1449

Di Berardino J, Marmagne A, Berger A, Yoshimoto K, Cueff G, Chardon F, Masclaux-Daubresse C, Reisdorf-Cren M (2018) Autophagy controls resource allocation and protein storage accumulation in Arabidopsis seeds. J Exp Bot **69**: 1403–1414

Djordjevic MA, Mohd-Radzman NA, Imin N (2015) Small-peptide signals that control root nodule number, development, and symbiosis. J Exp Bot **66**: 5171–5181

Gou X, He K, Yang H, Yuan T, Lin H, Clouse SD, Li J (2010) Genome-wide cloning and sequence analysis of leucine-rich repeat receptor-like protein kinase genes in *Arabidopsis thaliana*. BMC Genomics **11**: 19

Groszmann M, Bylstra Y, Lampugnani ER, Smyth DR (2010) Regulation of tissue-specific expression of SPATULA, a bHLH gene involved in carpel development, seedling germination, and lateral organ growth in Arabidopsis. J Exp Bot **61**: 1495–1508

Groszmann M, Chandler PM, Ross JJ, Swain SM (2020) Manipulating gibberellin control over growth and fertility as a possible target for managing wild radish weed populations in cropping systems. Front Plant Sci **11**: 190

Groszmann M, Paicu T, Alvarez JP, Swain SM, Smyth DR (2011) SPATULA and ALCATRAZ, are partially redundant, functionally diverging bHLH genes required for Arabidopsis gynoecium and fruit development. Plant J **68**: 816–829

Groszmann M, Paicu T, Smyth DR (2008) Functional domains of SPATULA, a bHLH transcription factor involved in carpel and fruit development in Arabidopsis. Plant J **55**: 40–52

Guan M, de Bang TC, Pedersen C, Schjoerring JK (2016) Cytosolic glutamine synthetase Gln1;2 is the main isozyme contributing to GS1 activity and can be up-regulated to relieve ammonium toxicity. Plant Physiol **171**: 1921–1933

Guan M, Moller IS, Schjoerring JK (2015) Two cytosolic glutamine synthetase isoforms play specific roles for seed germination and seed yield structure in Arabidopsis. J Exp Bot **66**: 203–212

Herridge RP, Day RC, Baldwin S, Macknight RC (2011) Rapid analysis of seed size in Arabidopsis for mutant and QTL discovery. Plant Methods **7**: 3

Hoai PTT, Tyerman SD, Schnell N, Tucker M, McGaughey SA, Qiu J, Groszmann M, Byrt CS (2020) Deciphering aquaporin regulation and roles in seed biology. J Exp Bot **71**: 1763–1773

Huault E, Laffont C, Wen J, Mysore KS, Ratet P, Duc G, Frugier F (2014) Local and systemic regulation of plant root system architecture and symbiotic nodulation by a receptor-like kinase. PLoS Genet **10**: e1004891

Imin N, Patel N, Corcilius L, Payne RJ, Djordjevic MA (2018) CLE peptide tri-arabinosylation and peptide domain sequence composition are essential for SUNN-dependent autoregulation of nodulation in *Medicago truncatula*. New Phytol **218**: 73–80

Karimi M, Inzé D, Depicker A (2002) GATEWAY vectors for Agrobacterium-mediated plant transformation. Trends Plant Sci **7**: 193–195

Kay P, Groszmann M, Ross JJ, Parish RW, Swain SM (2013) Modifications of a conserved regulatory network involving INDEHISCENT controls multiple aspects of reproductive tissue development in Arabidopsis. New Phytol **197**: 73–87

Kleinboelting N, Huep G, Kloetgen A, Viehoever P, Weisshaar B (2012) GABI-Kat SimpleSearch: New features of the Arabidopsis thaliana T-DNA mutant database. Nucleic Acids Res **40**: D1211–D1215

Ladwig F, Stahl M, Ludewig U, Hirner AA, Hammes UZ, Stadler R, Harter K, Koch W (2012) Siliques Are Red1 from Arabidopsis acts as a bidirectional amino acid transporter that is crucial for the amino acid homeostasis of siliques. Plant Physiol **158**: 1643–1655

Laffont C, Huault E, Gautrat P, Endre G, Kalo P, Bourion V, Duc G, Frugier F (2019) Independent regulation of symbiotic nodulation by the SUNN negative and CRA2 positive systemic pathways. Plant Physiol **180**: 559–570

Lea US, Slimestad R, Smedvig P, Lillo C (2007) Nitrogen deficiency enhances expression of specific MYB and bHLH transcription factors and accumulation of end products in the flavonoid pathway. Planta **225**: 1245–1253

Li F, Chung T, Pennington JG, Federico ML, Kaeppler HF, Kaeppler SM, Otegui MS, Vierstra RD (2015) Autophagic recycling plays a central role in maize nitrogen remobilization. Plant Cell **27**: 1389–1408

Liu C, Xue Z, Tang D, Shen Y, Shi W, Ren L, Du G, Li Y, Cheng Z (2018) Ornithine δ-aminotransferase is critical for floret development and seed setting through mediating nitrogen reutilization in rice. Plant J **96**: 842–854

Livak KJ, Schmittgen TD (2001) Analysis of relative gene expression data using real-time quantitative PCR and the $2^{-\Delta\Delta C_T}$ method. Methods **25**: 402–408

Ma X, Cheng Z, Qin R, Qiu Y, Heng Y, Yang H, Ren Y, Wang X, Bi J, Ma X, et al (2013) OsARG encodes an arginase that plays critical roles in panicle development and grain production in rice. Plant J **73**: 190–200

Martin A, Lee J, Kichey T, Gerentes D, Zivy M, Tatout C, Dubois F, Balliau T, Valot B, Davanture M, et al (2006) Two cytosolic glutamine synthetase isoforms of maize are specifically involved in the control of grain production. Plant Cell **18**: 3252–3274

Masclaux-Daubresse C, Chardon F (2011) Exploring nitrogen remobilization for seed filling using natural variation in Arabidopsis thaliana. J Exp Bot **62**: 2131–2142

Mohd-Radzman NA, Binos S, Truong TT, Imin N, Mariani M, Djordjevic MA (2015) Novel MtCEP1 peptides produced in vivo differentially regulate root development in *Medicago truncatula*. J Exp Bot **66**: 5289–5300

Mohd-Radzman NA, Laffont C, Ivanovici A, Patel N, Reid D, Stougaard J, Frugier F, Imin N, Djordjevic MA (2016) Different pathways act downstream of the CEP peptide receptor CRA2 to regulate lateral root and nodule development. Plant Physiol **171**: 2536–2548

Moison M, Marmagne A, Dinant S, Soulay F, Azzopardi M, Lothier J, Citerne S, Morin H, Legay N, Chardon F, et al (2018) Three cytosolic glutamine synthetase isoforms localized in different-order veins act together for N remobilization and seed filling in Arabidopsis. J Exp Bot **69**: 4379–4393

Müller B, Fastner A, Karmann J, Mansch V, Hoffmann T, Schwab W, Suter-Grotemeyer M, Rentsch D, Truernit E, Ladwig F, et al (2015) Amino acid export in developing Arabidopsis seeds depends on UmamiT facilitators. Curr Biol **25**: 3126–3131

Nisar N, Verma S, Pogson BJ, Cazzonelli CI (2012) Inflorescence stem grafting made easy in Arabidopsis. Plant Methods **8**: 50

Nunes C, O'Hara LE, Primavesi LF, Delatte TL, Schluepmann H, Somsen GW, Silva AB, Fevereiro PS, Wingler A, Paul MJ (2013) The trehalose 6-phosphate/SnRK1 signaling pathway primes growth recovery following relief of sink limitation. Plant Physiol **162**: 1720–1732

Ogilvie HA, Imin N, Djordjevic MA (2014) Diversification of the C-TERMINALLY ENCODED PEPTIDE (CEP) gene family in angiosperms, and evolution of plant-family specific CEP genes. BMC Genomics **15**: 870

Ohkubo Y, Tanaka M, Tabata R, Ogawa-Ohnishi M, Matsubayashi Y (2017) Shoot-to-root mobile polypeptides involved in systemic regulation of nitrogen acquisition. Nat Plants **3**: 17029

Okamoto S, Suzuki T, Kawaguchi M, Higashiyama T, Matsubayashi Y (2015) A comprehensive strategy for identifying long-distance mobile peptides in xylem sap. Plant J **84**: 611–620

Patel N, Mohd-Radzman NA, Corcilius L, Crossett B, Connolly A, Cordwell SJ, Ivanovici A, Taylor K, Williams J, Binos S, et al (2018) Diverse peptide hormones affecting root growth identified in the *Medicago truncatula* secreted peptidome. Mol Cell Proteomics **17**: 160–174

Patterson K, Cakmak T, Cooper A, Lager I, Rasmusson AG, Escobar MA (2010) Distinct signalling pathways and transcriptome response signatures differentiate ammonium- and nitrate-supplied plants. Plant Cell Environ **33**: 1486–1501

Perchlik M, Tegeder M (2018) Leaf amino acid supply affects photosynthetic and plant nitrogen use efficiency under nitrogen stress. Plant Physiol **178**: 174–188

Roberts I, Smith S, De Rybel B, Van Den Broeke J, Smet W, De Cokere S, Mispelaere M, De Smet I, Beeckman T (2013) The CEP family in land plants: Evolutionary analyses, expression studies, and role in Arabidopsis shoot development. J Exp Bot **64**: 5371–5381

Roberts I, Smith S, Stes E, De Rybel B, Staes A, van de Cotte B, Njo MF, Dedeyne L, Demol H, Lavenus J, et al (2016) CEP5 and XIP1/CEPR1 regulate lateral root initiation in Arabidopsis. J Exp Bot **67**: 4889–4899

Roy S, Lundquist P, Udvardi M, Scheible WR (2018) Small and mighty: Peptide hormones in plant biology. Plant Cell **30**: tpc.118.tt0718

Rubin G, Tohge T, Matsuda F, Saito K, Scheible WR (2009) Members of the LBD family of transcription factors repress anthocyanin synthesis and affect additional nitrogen responses in Arabidopsis. Plant Cell **21**: 3567–3584

Santiago J, Brandt B, Wildhagen M, Hohmann U, Hothorn LA, Butenko MA, Hothorn M (2016) Mechanistic insight into a peptide hormone signaling complex mediating floral organ abscission. eLife **5**: e15075

Santiago JP, Tegeder M (2016) Connecting source with sink: The role of Arabidopsis AAP8 in phloem loading of amino acids. Plant Physiol **171**: 508–521

Scheible WR, Morcuende R, Czechowski T, Fritz C, Osuna D, Palacios-Rojas N, Schindelasch D, Thimm O, Udvardi MK, Stitt M (2004) Genome-wide reprogramming of primary and secondary metabolism, protein synthesis, cellular growth processes, and the regulatory infrastructure of Arabidopsis in response to nitrogen. Plant Physiol **136**: 2483–2499

Schulze W, Schulze ED, Stadler J, Heilmeier H, Stitt M, Mooney HA (1994) Growth and reproduction of *Arabidopsis thaliana* in relation to storage of starch and nitrate in the wild-type and in starch-deficient and nitrate-uptake-deficient mutants. Plant Cell Environ **17**: 795–809

Shabala S, White RG, Djordjevic MA, Ruan YL, Mathesius U (2016) Root-to-shoot signalling: Integration of diverse molecules, pathways and functions. Funct Plant Biol **43**: 87–104

Shinohara H, Mori A, Yasue N, Sumida K, Matsubayashi Y (2016) Identification of three LRR-RKs involved in perception of root meristem growth factor in Arabidopsis. Proc Natl Acad Sci USA **113**: 3897–3902

Smyth DR, Bowman JL, Meyerowitz EM (1990) Early flower development in Arabidopsis. Plant Cell **2**: 755–767

Stadler R, Lauterbach C, Sauer N (2005) Cell-to-cell movement of green fluorescent protein reveals post-phloem transport in the outer integument and identifies symplastic domains in Arabidopsis seeds and embryos. Plant Physiol **139**: 701–712

Sui Z, Wang T, Li H, Zhang M, Li Y, Xu R, Xing G, Ni Z, Xin M (2016) Overexpression of peptide-encoding OsCEP6.1 results in pleiotropic effects on growth in rice (*O. sativa*). Front Plant Sci **7**: 228

Tabata R, Sumida K, Yoshii T, Ohyama K, Shinohara H, Matsubayashi Y (2014) Perception of root-derived peptides by shoot LRR-RKs mediates systemic N-demand signaling. Science **346**: 343–346

Takatani N, Ito T, Kiba T, Mori M, Miyamoto T, Maeda S, Omata T (2014) Effects of high CO_2 on growth and metabolism of Arabidopsis seedlings during growth with a constantly limited supply of nitrogen. Plant Cell Physiol **55**: 281–292

Taleski M, Imin N, Djordjevic MA (2016) New role for a CEP peptide and its receptor: Complex control of lateral roots. J Exp Bot **67**: 4797–4799

Taleski M, Imin N, Djordjevic MA (2018) CEP peptide hormones: Key players in orchestrating nitrogen-demand signalling, root nodulation, and lateral root development. J Exp Bot **69**: 1829–1836

Tegeder M, Masclaux-Daubresse C (2018) Source and sink mechanisms of nitrogen transport and use. New Phytol **217**: 35–53

Vidal EA, Gutiérrez RA (2008) A systems view of nitrogen nutrient and metabolite responses in Arabidopsis. Curr Opin Plant Biol **11**: 521–529

Wilkinson JQ, Crawford NM (1993) Identification and characterization of a chlorate-resistant mutant of *Arabidopsis thaliana* with mutations in both nitrate reductase structural genes NIA1 and NIA2. Mol Gen Genet **239**: 289–297